17th AIAA/CEAS Aeroacoustics Conference (32nd AIAA Aeroacoustics Conference)
05 - 08 June 2011, Portland, Oregon

AIAA 2011-2926

17th AIAA/CEAS Aeroacoustic Conference and Exhibit, 6-8 June 2010, Portland, Oregon

Farfield filtering of subsonic jet noise: Mach and Temperature effects

M. Kœnig*, A.V.G. Cavalieri†, P. Jordan‡, J. Delville§, Y. Gervais¶
Institut Pprime, Branche Fluide, UPR 3346, CNRS, Université de Poitiers, ENSMA, France

D. Papamoschou‖
Departement of Mechanical and Aerospace Engineering, University of California Irvine

We present an analysis of the sound field radiated by jets at different Mach numbers and temperature ratios. The methodology is similar to that developed by Kœnig *et al.*[1] in a previous study, where spatial and temporal structures of the sound field of a Mach 0.9 cold jet are filtered and analysed by means of Proper Orthogonal Decomposition and wavelet transform. Using both the POD and wavelet-filtered signals the acoustic field is decomposed into two components: a coherent structure (CS) component and a residuum (R). A source imaging procedure is then applied and the results compared with the CS component obtained by the two filtering operations.

The main results include the following observations. (1) While the shallow-angle acoustic spectra of isothermal jets scale best with Helmholtz number, those of the heated jets scale better with Strouhal number. This difference suggests that non-compact effects do not play as important a role in the heated jet where downstream radiation is concerned, contrary to what is observed in isothermal jets; this in turn suggests a change in acoustic wavelength associated with the temperature of the jet, implying that source interference occurs in the core of the flows, an idea consistent with an axially-extended wavepacket source. (2) While in the isothermal jets no change in intermittency is observed as the Mach number is varied, when the jet is heated increasing the Mach number engenders a *decrease* in intermittency in the acoustic field; we can conjecture from this that high Mach number hot jets comprise lower levels of source 'jitter' (cf. Cavalieri *et al.*[2]). (3) The CS acoustic signatures identified by both wavelet and POD filtering present wavepacket superdirectivity. (4) The trends identified by the source imaging, as a function of Mach number for isothermal and heated jets, are consistent both with known changes in the mean flow structure and the results of linear stability theory.

I. Introduction

Clear phenomenological descriptions of the mechanisms responsible for jet noise remain elusive, despite a significant number of clues contained in the farfield signature of a jet. Two interesting characteristics of jet noise are the angular dependance of the far-field power spectrum, and the tendential inversion that occurs with respect to the effect of temperature at Mach 0.7: above and below this value heating respectively decreases and increases the radiated sound power. The directivity has led to the idea that two statistically independent sources may be at work in isothermal flows,[3] while the temperature effect may be associated with the fact that momentum and entropy fluctuations, with which there can be associated two source terms, are in fact correlated (see Bodony & Lele[4]).

*PhD Student, Institut Pprime, 43 rue de l'aérodrome 86036 Poitiers, France
†PhD Student, Institut Pprime, 43 rue de l'aérodrome 86036 Poitiers, France
‡Research Scientist, Institut Pprime, 43 rue de l'aérodrome 86036 Poitiers, France
§Research Scientist, Institut Pprime, 43 rue de l'aérodrome 86036 Poitiers, France
¶Professor, Institut Pprime, 40 avenue du Recteur Pineau 86022 Poitiers, France
‖Professor, University of California Irvine, Irvine, CA, USA

In a recent paper, Kœnig *et al.*[1] proposed two kinds of filtering operation, intended as alternatives to the usual spectral analysis, for investigating the structure of the sound field radiated by subsonic jets. The first operation is a spatial filtering of the data using Proper Orthogonal Decomposition. The second involves a temporal filtering of the data via wavelet transform. As jet sources are known to display intermittency (see Juvé *et al.*,[5] Guj *et al.*,[6] Hileman *et al.*[7]), the wavelet transform as applied by Farge[8] is a useful tool to quantify this phenomenon.

In this paper, we apply the same analysis methodology as Kœnig *et al.*,[1] but this time we vary the Mach number and the temperature ratio of the jet. The Mach number effect is investigated for unheated and heated jets with the two filtering operations. Both filtering operations are used to isolate the component of the sound field associated with what is loosely referred to as coherent structures (CS), and this component is then compared with a wavepacket sound source *ansatz*. Source imaging, based on this kind of ansatz, is used to explore how the wavepacket parameters change as a function of Mach number and temperature ratio.

The paper is organised as follows. In section II the experimental setup is described. This is followed by an outline of the analysis procedure in section III. Section IV contains a presentation of the effect of changing the Mach number for isothermal jets. We here observe that the shallow-angle sound spectra scale best with Helmholtz number, suggests that the associated sources are non-compact. The CS components obtained by both the POD and wavelet filters, sensitive, respectively, to the spatial and temporal structure of the sound field, are found to be consistent with wavepacket sources: they present 'peaky' spectra and are superdirective. In section V the same analysis is reported for a heated jet. Two interesting differences between hot and isothermal jets are here observed: (1) the heated jet shallow-angle spectra scale better with Strouhal number than with Helmholtz number. This difference suggests that non-compact effects do not as important a role in heated jets where downstream radiation is concerned, contrary to what is observed in isothermal jets; this in turn suggests a change in acoustic wavelength associated with the temperature of the jet, implying that source interference occurs in the core of the flows, an idea consistent with an axially-extended wavepacket source. (2) when the jet is heated, increasing the Mach number engenders a *decrease* in intermittency in the acoustic field, contrary to the isothermal result; we can conjecture from this that high Mach number hot jets comprise lower levels of source 'jitter' (cf. Cavalieri *et al.*[2]). Finally, in section VI the source imaging analysis is presented, and the dependence of the wavepacket parameters on Mach number, for both iosthermal and heated jets, is assessed. The trends observed are consistent with both know changes in the mean flow structure and the results of linear stability theory.

II. Experiment

A. Test facility and microphone array

The experiments were performed at the MARTEL facility of the Pprime Institute, CEAT (Centre d'Etudes Aérodynamiques et Thermiques), Poitiers, France on a 0.05 m diameter jet in a acoustic Mach number range of 0.6 to 1.0 and a temperature ratio range of 1.0 to 2.0. The jet Reynolds number was approximately 10^6.

The acoustic field was sampled using an arc of 12 microphones at a distance of 30 diameters from and centered on the jet exit. The angular position of the microphones varies from 30° to 140° with respect to the downstream jet axis. The acoustic setup is shown in figure 1. For further details about the experiments, see Jordan & Gervais.[9]

B. Test matrix

The nine test points are summarised in table 1. The Mach number range extends from 0.60 to 1.00. Considering the convective Mach number $M_c = 0.6 \times M_a$, it spans a range of 0.36 to 0.60. Unheated and heated jet are investigated. The temperature ratio ranges from 1.0 to 2.0. In this study we explore the effect of varying the Mach number in both isothermal and heated ($T_j/T_a = 2$) conditions.

III. Analysis procedure

We decompose the farfield of the jet by appealing to both its spatial (polar) and temporal structures, as per Kœnig *et al.*[1] Once again, the operations are achieved by means of a Proper Orthogonal Decomposition (POD) and a wavelet transform.

Figure 1. Acoustic measurement setup.

Case Number	T_j/T_a	M_a	M_j	Q_m [kg/s]
1	1.0	0.60	0.600	0.483
2	1.0	0.75	0.750	0.604
3	1.0	0.90	0.900	0.725
4	1.5	0.60	0.490	0.322
5	1.5	0.75	0.612	0.403
6	1.5	0.90	0.735	0.483
7	2.0	0.75	0.530	0.302
8	2.0	0.90	0.636	0.362
9	2.0	1.00	0.707	0.403

Table 1. Test matrix for farfield measurements.

A. Proper Orthogonal Decomposition

We use spectral POD to decompose the sound field. The kernel of the POD problem is the cross-spectral matrix $G(\theta_i, \theta_j, \omega)$:

$$G(\theta_i, \theta_j, \omega) =< p(\theta_i, \omega) p^*(\theta_j, \omega) >, \tag{1}$$

where $< . >$ denotes ensemble averaging. The Fredholm integral is solved one frequency at a time, providing us with frequency-dependent eigenvalues and eigenvectors. The spatial phase of the soundfield is captured at each frequency, and this information is contained in the shapes of the eigenfunctions (which are complex). The temporal phase is lost, but it can be recovered later by projecting the original data onto the eigenfunctions.

As in Kœnig *et al.*,[1] based on the directivity of the POD modes, the farfield is decomposed in a component which we attribute to coherent structures (CS) and a residuum (R). We retain the first POD mode as our CS component, the remaining modes being lumped together to form the residuum:

$$p_{CS}(\theta, t) = p(\theta, t)^{(1)} \quad \text{and} \quad p_R(\theta, t) = \sum_{k=2}^{N_{mod}} p(\theta, t)^{(k)}. \tag{2}$$

B. Wavelet transform

The continuous wavelet transform has proved useful for extracting the signature of high-energy, temporally-localised events. The equations used to perform such a transformation are here briefly presented. For more information the reader can refer to Farge.[8] The continuous wavelet transform of the pressure signal is:

$$\tilde{p}(s,t) = \int_{-\infty}^{\infty} p(\tau)\psi(s,t-\tau)d\tau, \tag{3}$$

where s is the scale of the wavelet function. A Paul wavelet is used in this study, defined for $s = 1$ with an order m as (see Torrence *et al.*[10] for more details):

$$\psi(1,t-\tau) = \frac{2^m i^m m!}{\sqrt{\pi(2m)!}}[1-i(t-\tau)]^{-(m+1)}. \tag{4}$$

Other kinds of wavelet families were investigated in a previous study,[1] and the following intermittency metric was found to give most insight regarding the structure of the farfield:

Global Intermittency Measure

The Global Intermittency Measure (GIM)[1] allows us to identify temporally-, or scale-localised events that make large contributions to the overall fluctuation energy. The following filtering operation is effected:

$$\tilde{p_f}(\theta,s,t) = \begin{cases} \tilde{p}(\theta,s,t) & \text{if } |\tilde{p}(\theta,s,t)|^2 > \alpha \\ 0 & \text{if } |\tilde{p}(\theta,s,t)|^2 < \alpha \end{cases} \tag{5}$$

The parameter α, which can be see as a threshold value, has units of energy density in the wavelet domain. An inverse wavelet transform of the resulting filtered wavelet pressure gives the CS component. The R component is the difference between the baseline and the CS time pressure signals.

IV. Mach number effect for an isothermal jet

In this section, we focus on the first three cases. The jet considered is isothermal with an acoustic Mach number varying from 0.60 to 0.90. After discussing the different baseline spectra, we decompose the far-field pressure with the POD and wavelet filters.

A. Spectral shapes and velocity dependance of baseline spectra

The spectra have been scaled by setting their respective maximum to 0dB (no shift in frequency is effected). This operation allows us to compare the differences between spectral shapes at different angles.

Figure 2 presents the results of the scaling at 30° as a function of (a) the Helmholtz number (defined as $He = fD/c_\infty$) and (b) the Strouhal number (defined as $St = fD/U$). Best collapse is obtained when scaled using the Helmholtz number (similar observations were made by Lush[11] and Tanna[12]), an indication that source radiating to shallow polar angles is non-compact (see Cavalieri *et al.*[13] for further discussion).

Figures 2(c) and (d) present the results of the scaling for the 90° spectra. We should note that the sound spectrum of the Mach 0.6 jet is contaminated with installation noise in the range $1 < St < 2$, however the basic trend can nonetheless be discerned. While the result is not quite as clear as for the shallow polar angles, the Helmholtz scaling appears to be a little better , particularly in the lower frequencies.

Figure 3 presents the directivity for different Mach numbers in term of OASPL and SPL for St=0.2. The directivity is more pronounced at higher Mach numbers especially when we consider spectral peaks at St=0.2. In this case, we have a rapid falloff of SPL in the range $30° < \theta < 60°$. The maximum fall of SPL observed is at Mach 0.9 where a decrease of more than 13 dB is observed between SPL at 30° and SPL at 60°.

B. POD filter

The CS component is here considered to correspond to the first POD mode, following the observations of Kœnig *et al.*[1] The filtered CS spectra have been scaled for the three Mach numbers 0.60, 0.75 and 0.90, as

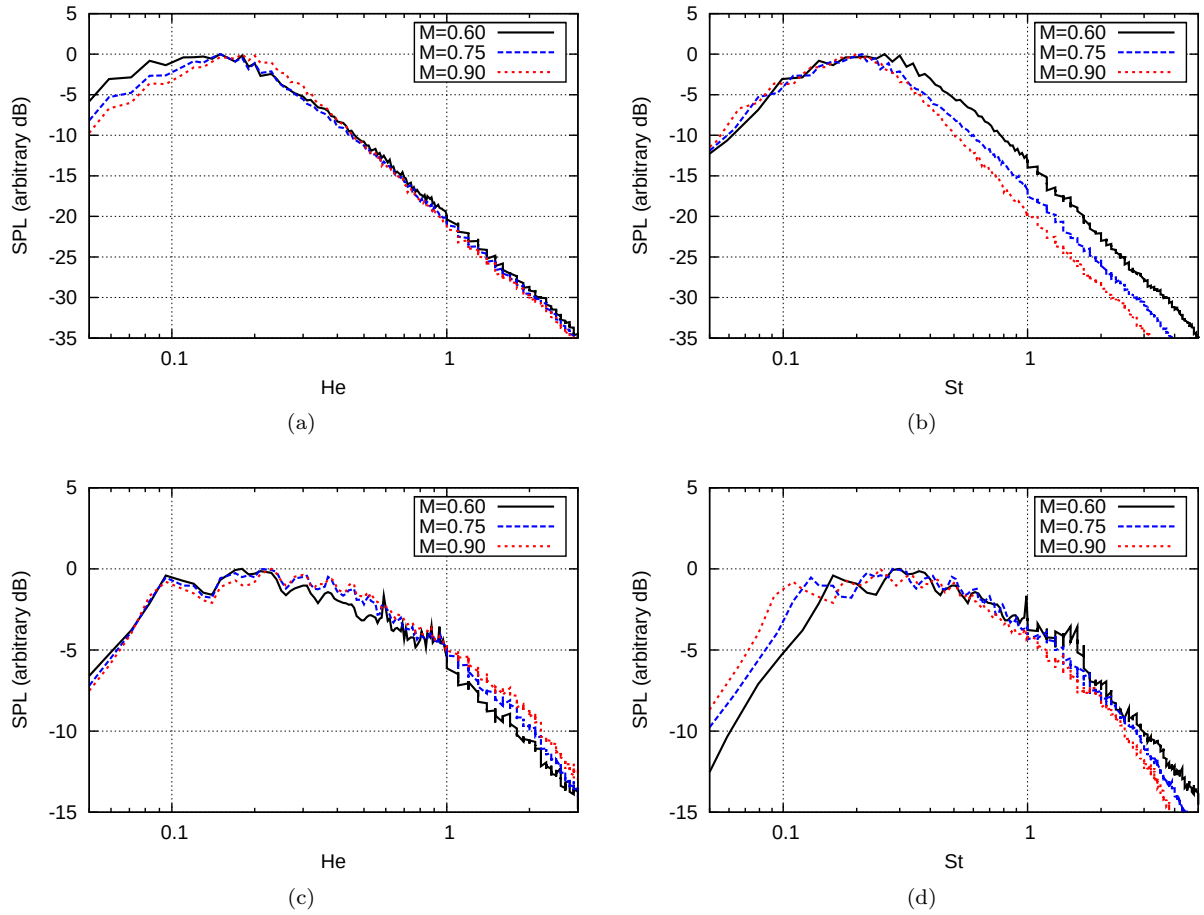

Figure 2. Spectral shapes for isothermal jets at different Mach numbers, scaled with Helmholtz and Strouhal numbers. (a) and (b): θ=30°; (c) and (d) and θ=90°

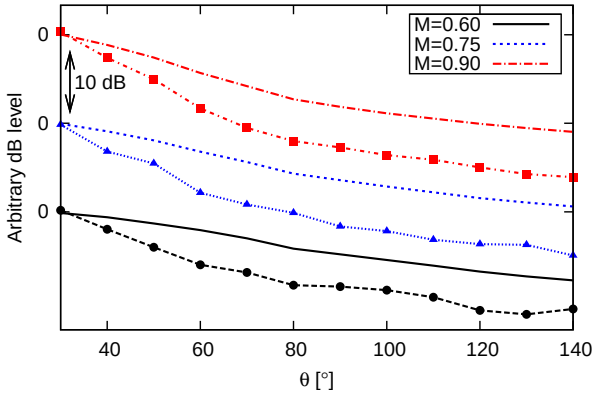

Figure 3. Directivity for different Mach numbers ; lines without symbols : OASPL ; lines with symbols: SPL at St=0.2 for different Mach numbers.

in section A, by both Helmholtz and Strouhal numbers. Figure 4(a) and (b) compares the spectral shapes at 30°.

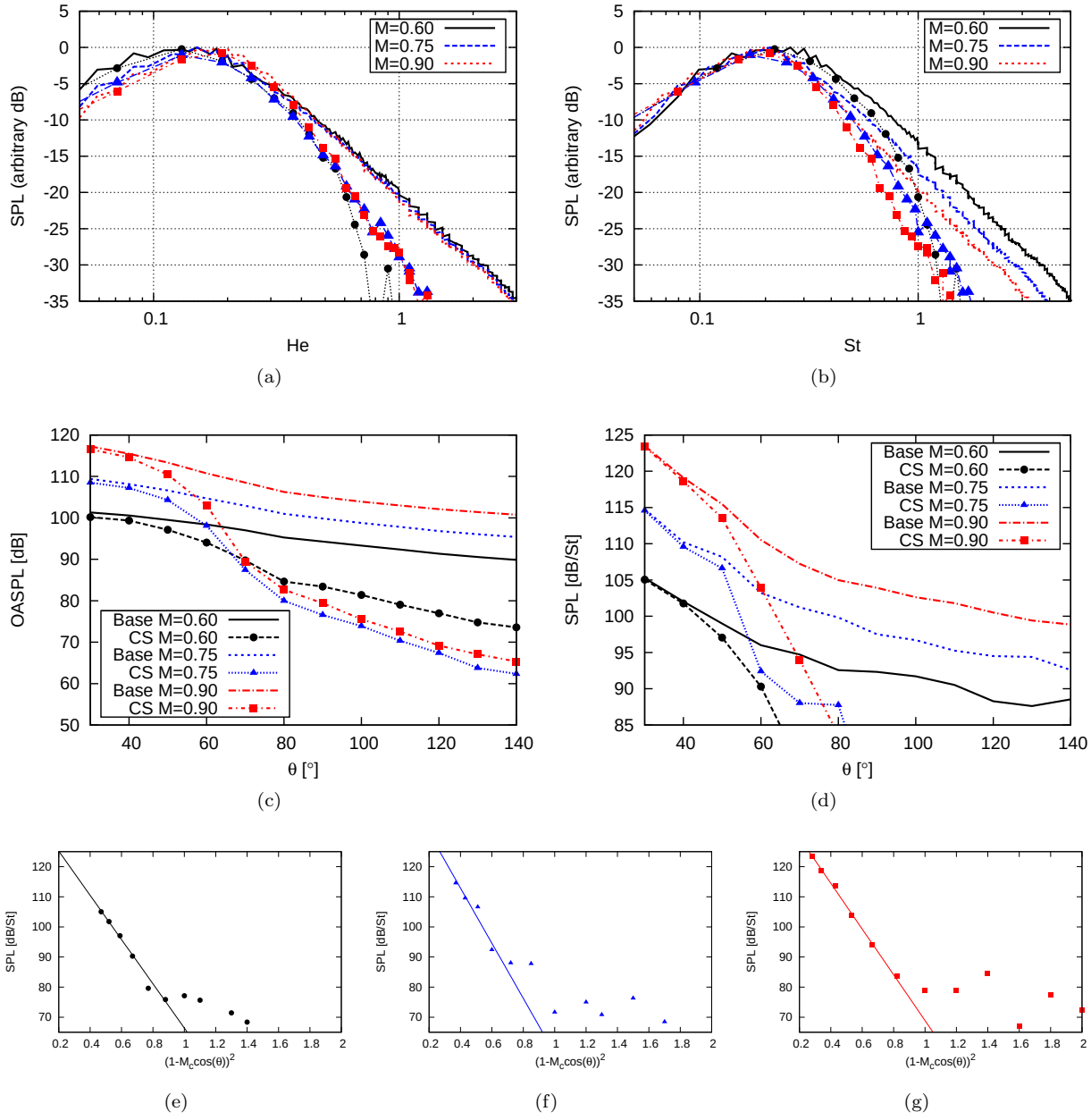

Figure 4. Spectral shapes at θ=30°and directivities for POD CS component of sound field of isothermal jets at different Mach numbers. (a) Spectra scaled by Helmholtz number; (b) Spectra scaled by Strouhal number; (c) Comparison of OASPL of total sound field and CS component; (d) Comparison of SPL, for St=0.2, of total sound field and CS component. Superdirectivity of the CS component for (a) Mach 0.60, (b) Mach 0.75 and (c) Mach 0.90.

As in the baseline case, the spectra scale best with Helmholtz number in spite of the sudden fall of the Mach 0.6 CS spectrum in high-frequencies ($St > 1$).

Figures 4(c) and (d) show the directivity for different Mach numbers in term of OASPL and SPL for St=0.2 for the different baseline and CS component. Regardless of the Mach number, the CS component is always more directive, showing a directivity that resembles that of a wavepacket. It is also interesting to note that the directivity of the CS component is more pronounced at higher Mach numbers suggesting

that the POD filter does not act in the same way at Mach 0.60 and Mach 0.90: the POD filter appears to capture the progressive emergence of a highly directive, wavepacket-like signature. Further discussion on this phenomenon can be found in Cavalieri *et al.*[13]

Previous studies by Crow,[14] Crighton[15] or Ffowcs-Williams & Kempton,[16] propose a wavepacket model to represent the source mechanism comprised by coherent structures. The source is represented as an axial distribution of axially-aligned longitudinal quadrupoles of the form:

$$T_{11}(\vec{y},\tau) = 2\rho_0 U\tilde{u}\frac{\pi D^2}{4}\delta(y_2)\delta(y_3)e^{i(\omega\tau - ky_1)}e^{-\frac{y_1^2}{L^2}}. \tag{6}$$

This source comprises a convected wave with frequency ω, wavenumber k and which is modulated by a gaussian. M_c is the Mach number based on the phase velocity U_c (which was assumed as $U_c = 0.6 \times U_j$) of the convected wave. Such a source generates a sound field of the form

$$p(\vec{x},t) = -\frac{\rho_0 U\tilde{u}M_c^2(kD^2)L\sqrt{\pi}\cos^2\theta}{8|\vec{x}|}e^{-\frac{L^2k^2(1-M_c\cos\theta)^2}{4}}e^{i\omega(t-\frac{|\vec{x}|}{c})}. \tag{7}$$

The sound intensity decays exponentially with $(1 - M_c\cos\theta)^2$, a behaviour labeled as superdirectivity (see Crighton & Huerre[17]). The superdirective character of the CS component educed by the POD filter is demonstrated in figure 4(e-g), where the SPL at St=0.2 is plotted as a function of $(1-M_c\cos\theta)^2$; exponential decay (indicated by the straight lines) is indeed observed for low angles, with decays of up to 30dB. We conclude that the CS component of the sound field extracted by the POD filter can be considered as the signature of a wavepacket source mechanism.

C. Wavelet filter

The wavelet transform and filtering is performed as outlined in section III.B. Total energy is conserved under the wavelet transform and there exists the following equivalent of Parseval's theorem[10] for a given pressure signal localized at the angle θ :

$$\int_{\mathbb{R}}|p(t)|^2dt = C_\psi^{-1}\int_{\mathbb{R}^+}\int_{\mathbb{R}}|\tilde{p}(s,t)|.|\tilde{p}^*(s,t)|\frac{dsdt}{s^2} \tag{8}$$

where $p(t)$ is the time pressure signal for a given polar position θ, $\tilde{p}(s,t)$ its continuous wavelet transform and C_ψ is a constant associated with the wavelet function which we use. Calculation of the energy after GIM filtering, using equation 8, gives the ratio of energy conserved to total energy.

The analysis here comprises two steps. We first vary the filter threshold and study the ratio of energy conserved to total energy as a function the threshold value. We then choose a single threshold value, $\alpha = 0.00015$ (which retains of the order of 60% of the signal energy), chosen because it corresponds to a filtering that leads to an asymptotic, 'peaky', spectral shape; we consider the signal thus filtered to correspond to a CS component of the soundfield, this time obtained with respect to a criterion based on the temporal intermittency of the microphone signals. We proceed to study the spectra and directivity of this filtered signal.

The result of varying the threshold is shown in figure 5. The shapes of these curves are taken as a measure of the signal 'burstiness' or intermittency: a curve that decays rapidly with increasing α contains fewer temporally-localised events making significant contributions to the overall energy, whereas a curve that decays more slowly with α indicates a greater contribution to the overall energy from such temporally-localised events. Kœnig *et al.*[1] showed that GIM filtering produces two families of curves. At low angles (30°, 40° and 50°), the curves indicate signals characterised by high levels of energetic intermittency; at higher angles ($\theta \geq 60°$), all the signals are characterised by similarly low levels of energetic intermittency.

In this paper we concentrate on the low-angle family and study the effect of changing the Mach number. The result is shown in figure 5. It is possible to conclude that the Mach number does not significantly modify the intermittency of the sound field when the jet remains isothermal. We will see that *this is not the case when the jet is heated.*

The filtered CS spectra are again scaled by the Helmholtz number and the Strouhal number. Figures 6(a) and (b) show filtered spectra at 30° with α=0.00015. As for the baseline case, there is again better collapse of the CS spectral shapes when they are scaled with the Helmholtz number. In this case, the spectral

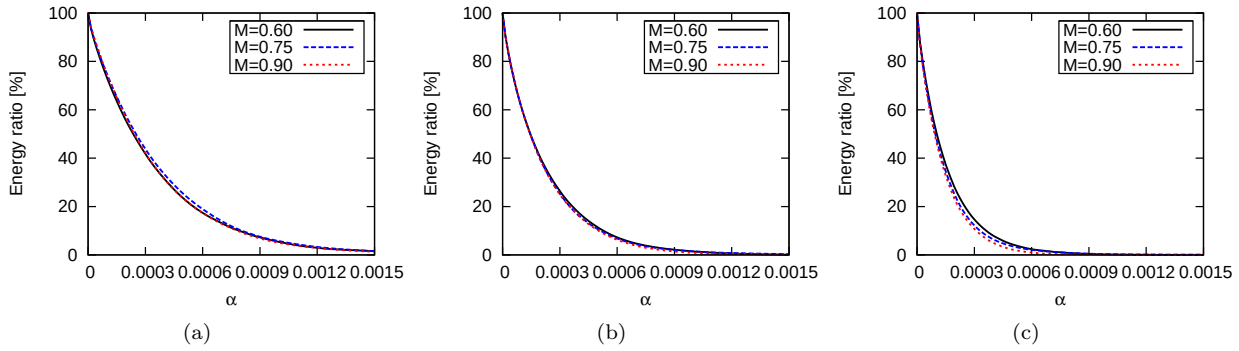

Figure 5. Energy ratio (filtered/residuum) as a function of Mach number; (a) 30°; (b) 40°; (c) 50°.

shape of the CS component is close to the shape of the axisymmetric mode of the jet (see Cavalieri *et al.*[13] for details).

The OASPL and SPL directivities of the baseline and the wavelet-CS component are plotted in figure 6(c) and (d) for different Mach numbers. Both are clearly more directive than the baseline case. Contrary to the POD filter, the wavelet filter acts in a similar manner whatever the Mach number, particularly so at higher emission angles.

As in the POD section, the superdirectivity of the CS component is analysed in figures 6(e-f) for $\alpha = 0.00015$. The CS component again displays superdirectivity, consistent with a wavepacket source.

V. Mach number effect for a heated jet

In this section we repeat the analysis for a heated jet with temperature ratio equal to 2.0 and an acoustic Mach number varying from 0.75 to 1.00. The same methodology is followed: following a presentation of the baseline spectra, we apply POD and wavelet filtering.

A. Spectral shapes and velocity dependance of baseline spectra

As in section IV, the spectral shapes for different jet exit velocities (Mach 0.75, 0.90 and 1.00) are set for a maximum at 0dB and scaled with both Helmholtz and Strouhal numbers. The results are presented in figure 7.

Contrary to the isothermal case, the scaling with the Helmholtz number does not provide a collapse of the curves at 30°, a better collapse being obtained with the Strouhal number. This quite different scaling suggests that the heated jet is a more compact source than its isothermal counterpart. If we consider, once again, the sound source in terms of an axially-aligned wavepacket, this difference can be explained by virtue of the fact that while the turbulence space-scales, convection velocities and associated time scales are of the same order of magnitude in both hot and isothermal jets (differences of no more than ten per cent should be expected in any of these characteristic quantities), the corresponding sound wavelength at the heart of the heated flow is 40% higher that of the isothermal flow. So, while characteristic scales of the axially-extended wavepacket remain of the same order of magnitude in both heated and isothermal flows, the change in sound speed at the heart of the heated flow causes the wavepacket in the hot jet to become increasingly compact as the jet temperature increases; this also suggests that the interference mechanisms leading to wavepacket radiation occur within the hot part of the jet, rather than towards the outer jet periphery.

B. POD filter

The CS component is again associated with the first POD mode. The filtered CS spectra have been scaled for the three Mach numbers, 0.75, 0.90 and 1.00 in a similar manner to that of section A. Once again, the results are presented scaled by both Helmholtz and Strouhal numbers. Figure 9(a) and (b) compares the spectral shapes at 30°. Best collapse of the spectral shapes is again obtained when spectra are scaled with the Strouhal number.

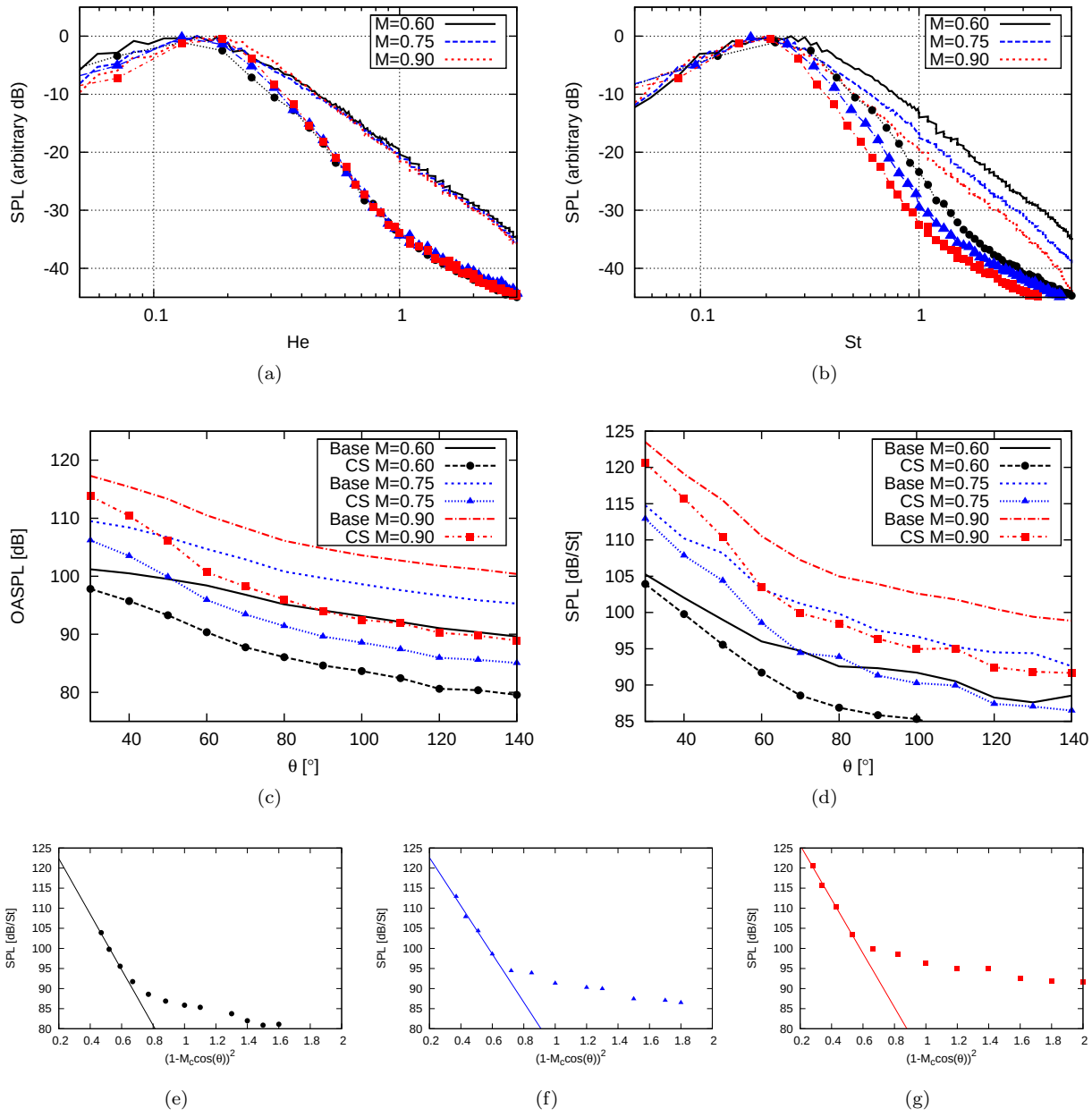

Figure 6. Spectral shapes at θ=30°and directivities for wavelet CS component of sound field of isothermal jets at different Mach numbers. (a) Spectra scaled by Helmholtz number; (b) Spectra scaled by Strouhal number; (c) Comparison of OASPL of total sound field and CS component; (d) Comparison of SPL, for St=0.2, of total sound field and CS component. Superdirectivity of the CS component for α=0.00015 and (a) Mach 0.60, (b) Mach 0.75 and (c) Mach 0.90.

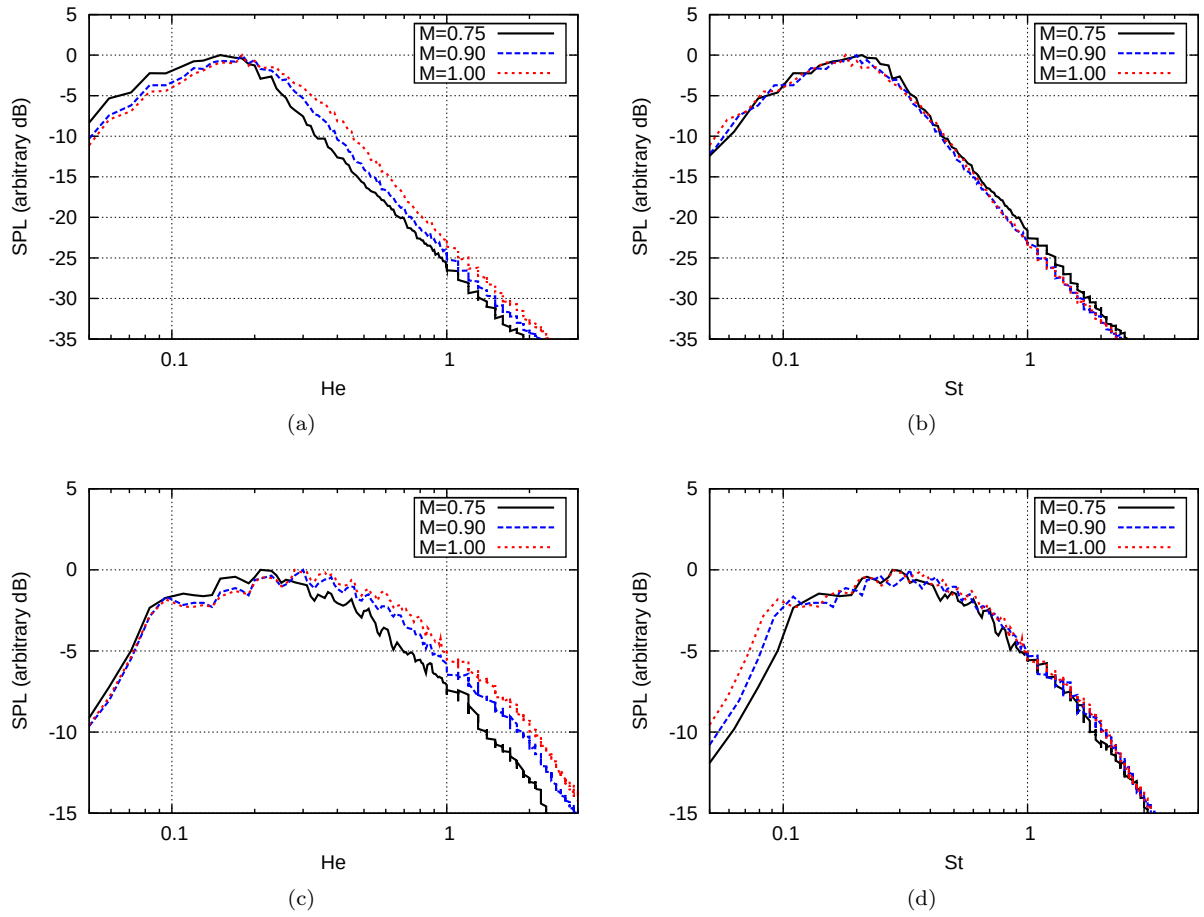

Figure 7. Spectral shapes for heated jets at different Mach numbers, scaled with Helmholtz and Strouhal numbers. (a) and (b): θ=30°; (c) and (d) and θ=90°

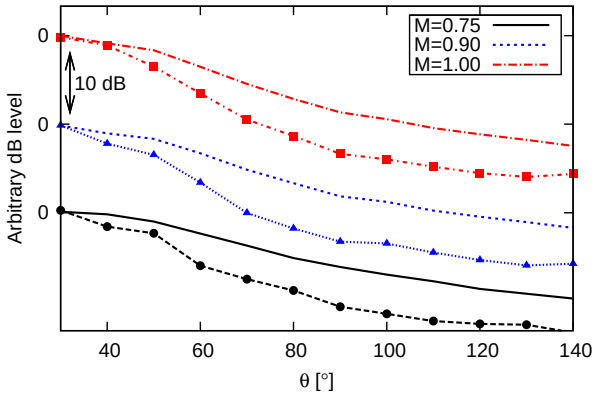

Figure 8. Directivity of heated jets for different Mach numbers ; lines without symbols: OASPL,; lines with symbols: SPL at St=0.2 for different Mach numbers.

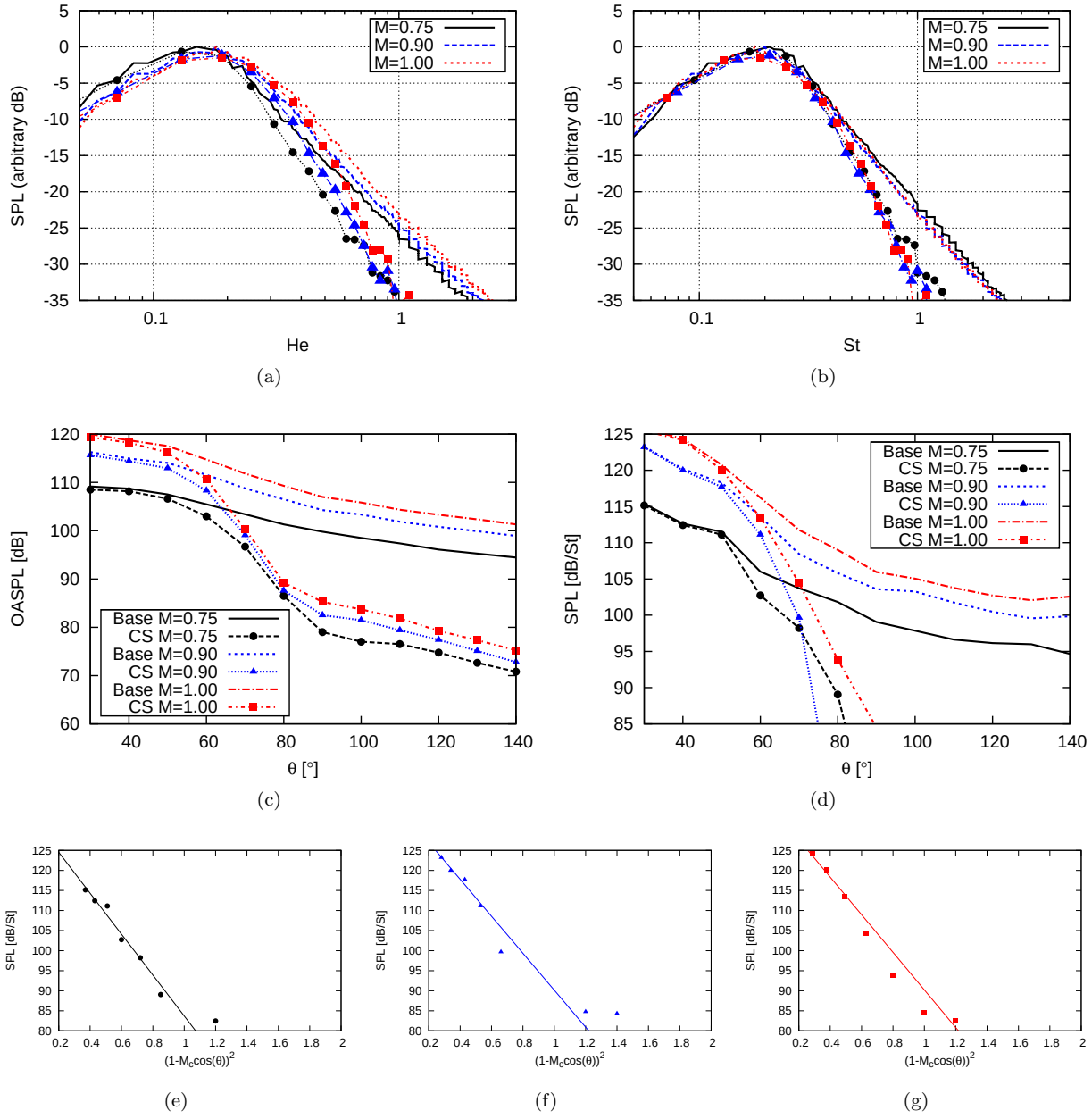

Figure 9. Spectral shapes at θ=30°and directivities for POD CS component of sound field of heated jets at different Mach numbers. (a) Spectra scaled by Helmholtz number; (b) Spectra scaled by Strouhal number; (c) Comparison of OASPL of total sound field and CS component; (d) Comparison of SPL, for St=0.2, of total sound field and CS component. Superdirectivity of the POD CS component: (e) Mach 0.75, (f) Mach 0.90 and (g) Mach 1.00.

Figure 9 presents the directivity for different Mach numbers in term of (c) OASPL and (d) SPL for St=0.2 for the different baseline and CS component. As for the unheated case, the CS component remains highly directive whatever the Mach number and its directivity has a shape—though a little less clear than the isothermal dlow—characteristic of a wavepacket type source (Figure 9(e-g)).

C. Wavelet filter

Varying the threshold of the wavelet filter, we obtain energy ratio curves that characterise the level of intermittency for a GIM filtering. Figure 10 shows the relationship between filtered energy and α at different Mach numbers for (a) θ=30°, (b) θ=40° and (c) θ=50°.

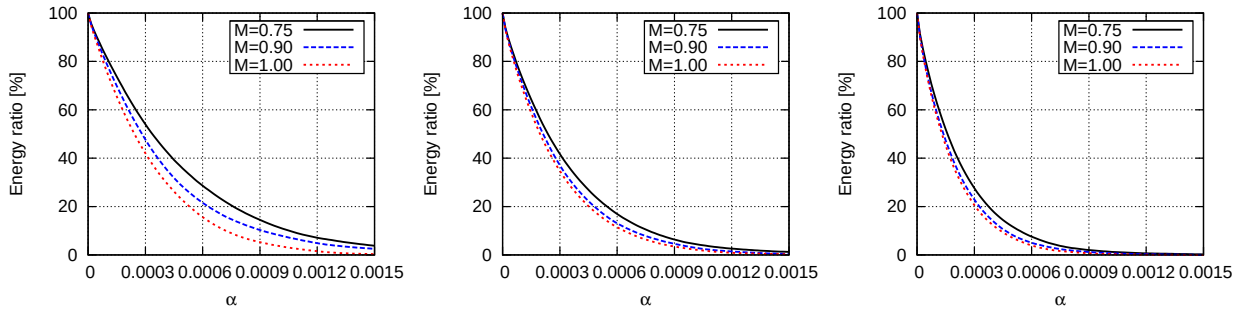

Figure 10. Energy ratio (filtered/residuum) as a function of Mach number; (a) 30°; (b) 40°; (c) 50°.

We see that, contrary to the isothermal jets, the intermittency of the sound field radiated by the heated jet *decreases with increasing Mach number*. This suggests that when the Mach number of a heated jet is increased, the source 'jitter' is reduced. Such 'jitter' has been shown by Cavalieri *et al.*[2] to be a source parameter to which the farfield shows high sensitivity. This decrease in intermittency with increasing Mach number in heated jets may therefore be related to the fact that at higher Mach numbers heating a jet reduces its noise. This points merits further exploration.

The filtered CS spectra has been scaled, for the three Mach numbers 0.75, 0.90 and 1.00, by both Helmholtz and Strouhal numbers. Figure 11(a) and (b) compares the spectral shapes at 30° for α=0.00015.

As was the case with for the baseline spectra, the CS spectra collapse when they are scaled with respect to the Strouhal number. The differences manifest in the baseline data persist after filtering into the CS component. The directivity of the CS component is again analysed in figure 11(e-g) for $\alpha = 0.00015$. The straight lines represent exponential decay. The CS component is again observed to display wavepacket superdirectivity.

VI. Imaging techniques

Source imaging techniques are useful in providing insight regarding source mechanisms (cf. Papamoschou[18] for example), provided: (1) the ansatz used bears some similarity to the source mechanism; (2) the algorithm converges on a parameter set that is physically realistic. As we observed wavepacket signatures for the filtered CS components (POD and wavelet) in the previous sections, we now use source imaging with a wavepacket 'ansatz' on the original database to quantify the Mach and temperature effects on the wavepacket source found by the minimisation algorithm.

The procedure goes as follows. The cross-spectrum $< Q(\vec{y},\omega)Q^*(\vec{y}\,',\omega)) >$ of the sound source field is described in terms of a parameter vector A_k which is determined by "matching" the modelled and measured acoustics. The matching involves the cross-spectral matrix $G(\vec{x}_m,\vec{x}_n,\omega)$ where $\vec{x}_m$ and $\vec{x}_n$ denote the spatial locations of measurement points m and n, respectively. The experimental measurement of the CSM is denoted G_{exp}. The modeled CSM is $G_{mod}(A_k,\vec{x}_m,\vec{x}_n,\omega)$, that is, it depends on the parameter vector A_k that describes the source model. Ideally, we would obtain A_k by setting :

$$G_{exp}(\vec{x}_m,\vec{x}_n,\omega) = G_{mod}(A_k,\vec{x}_m,\vec{x}_n,\omega) \tag{9}$$

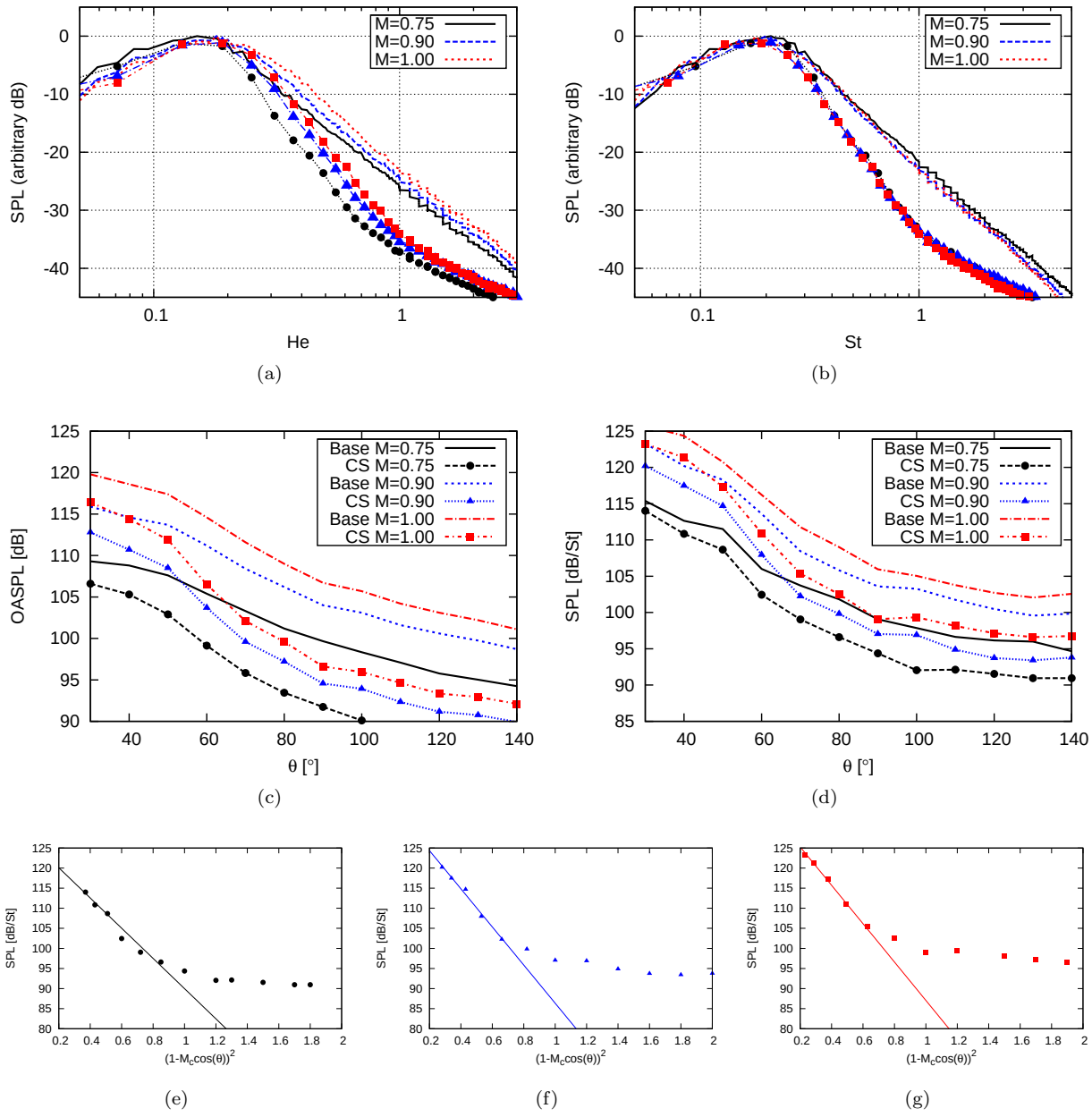

Figure 11. Spectral shapes at θ=30°and directivities for wavelet CS component of sound field of heated jets at different Mach numbers. (a) Spectra scaled by Helmholtz number; (b) Spectra scaled by Strouhal number; (c) Comparison of OASPL of total sound field and CS component; (d) Comparison of SPL, for St=0.2, of total sound field and CS component. Superdirectivity of the POD CS component: (e) Mach 0.75, (f) Mach 0.90 and (g) Mach 1.00.

and hope for an exact solution for A_k. This is rarely the case, so we instead resort to methods that minimise the difference between the modelled and measured acoustic fields. Concentrating on a given frequency ω, we define the error :

$$F(A_k) = \sum_{m,n=1}^{M} |G_{exp}(\vec{x}_m, \vec{x}_n) - G_{mod}(A_k, \vec{x}_m, \vec{x}_n)|^2 \tag{10}$$

where M is the total number of measuring stations. We seek a vector A_k that minimizes $F(A_k)$. A method that has proven effective is the conjugate gradient minimization method, particularly as implemented by Shanno and Phua.[19]

To calculate the modeled CSM, we consider a cylindrical surface of radius $r = r_0$ surrounding an axisymmetric jet. The pressure on the cylindrical surface is then prescribed as follows:

$$p(r_0, x, t) = p_0(x, A_k)e^{-i\omega t} \tag{11}$$

where $p_0(x, A_k)$ is an oscillatory function that amplifies and decays with x. For a given frequency ω and radius R, the modeled CSM is (see for instance Morris[20]):

$$G_{mod}(A_k, \theta_m, \theta_n) = \frac{1}{\pi R^2} \frac{\hat{p}_0(\frac{\omega}{c_\infty}\cos\theta_m, A_k)\hat{p}_0^*(\frac{\omega}{c_\infty}\cos\theta_n, A_k)}{H_0^{(1)}(\frac{\omega}{c_\infty}r_0\sin\theta_m)H_0^{(2)}(\frac{\omega}{c_\infty}r_0\sin\theta_n)}. \tag{12}$$

Asymmetric wavepacket *ansatz*

The wave source model is, in this case, simply a wavepacket like those in Crighton and Huerre.[17] On cylindrical surface $r = r_0$, the pressure is prescribed as follows :

$$p(r_0, x, t) = p_0(x, A_k)e^{-i\omega t}, \tag{13}$$

where $p_0(x, A_k)$ is an oscillatory function that amplifies and decays with x. We select an "asymmetric Gaussian" formulation for $p_0(x, A_k)$:

$$p_0(x, A_k) = \epsilon B(x)e^{i\alpha k}, \tag{14}$$

with $B(x)$ being a piecewise-defined function:

$$B(x) = \begin{cases} \exp(-b_1(x - x_0)^2), & x \le x_0 \\ \exp(-b_2(x - x_0)^2), & x > x_0 \end{cases}. \tag{15}$$

The vector A_k is composed of five parameters (ϵ, α, b_1, b_2, x_0) characteristics of an asymmetric Gaussian curve as we can see on figure 12.

An analytical solution for $\hat{p}_0(k)$ is:

$$\hat{p}_0(k) = \frac{\epsilon\sqrt{\pi}}{2}e^{ix_0(k-\alpha)}\Big(\frac{1}{\sqrt{b_2}}W(\beta_2) + \frac{1}{\sqrt{b_1}}W^*(\beta_1)\Big). \tag{16}$$

with $\beta_1 = \frac{k-\alpha}{\sqrt{b_1}}$, $\beta_2 = \frac{k-\alpha}{\sqrt{b_2}}$ and $W(x) = e^{-x^2}\mathrm{erfc}(ix)$ the Faddeeva function.

We explore the effect Mach number for both isothermal and heated jets, using the source imaging algorithm, assessing, in each case, how the wavepacket parameters vary as the Mach number and temperature are varied.

A. Dependence of wavepacket parameters on Mach number for isothermal jet

We consider the isothermal jet, $T_j/T_a = 1$, at the three Mach numbers, 0.6, 0.75 and 0.9 (see table 1). Figure 13 presents the results.

The main trends observed, as the Mach number is increased, comprise:

- A displacement of the wavepacket in the downstream direction. This is consistent with the lengthening L_{pc} of the potential core at higher Mach (see the formula $L_{pc}/D = 4.2 + 1.1M^2$ proposed by Lau *et al.*[21]), although the values obtained for the low frequency components seem a little exagerated.

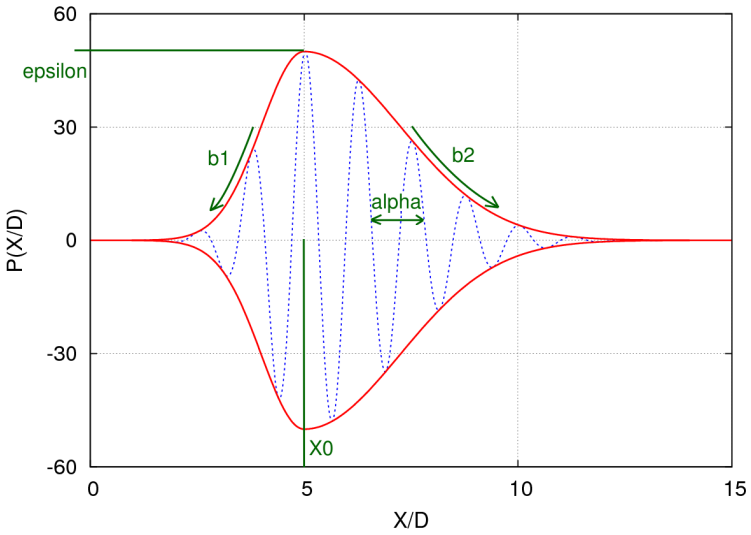

Figure 12. Asymmetric Gaussian curve used for the wavepacket model.

- The convection velocity decreases slightly; this is consistent with the trend predicted by linear stability theory (LST: cf. Michalke[22]).
- The wavepacket amplitude for the $M = 0.9$ case is not consistent with LST. This is possibly an artefact of the imaging algorithm, due to the fact that the microphone array used here is not entirely adapted to the problem, on account of the highly directional nature of the wavepacket sources. It is known that source imaging can produce such spurious results.
- No dramatic change is observed concerning the slopes, gaussian wavepacket 'ansatz' are obtained in particular, which is contrary to the results obtained by Papamoschou.[23] Once again, this behaviour may be due to the microphone array configuration.
- The directivity of the wavepacket source identified by the imaging is superdirective, in agreement with the CS signatures identified by the POD and wavelet filtering operations performed in the previous sections.

B. Dependence of wavepacket parameters on Mach number for heated jet

We consider the heated jet, $T_j/T_a = 2$, at the three Mach numbers, 0.75, 0.9 and 1 (see table 1). Figure 14 summarises the results.

The main trends observed here, as the Mach number is increased, comprise:

- A displacement of the wavepacket in the downstream direction. This, again, is consistent with the lengthening of the potential core at higher Mach.
- The convection velocity decreases slightly, again consistent with the trend predicted by linear stability theory.
- Apart from what looks like a spurious result at $St = 0.25$, the wavepacket amplitude does not vary as strongly with the Mach number as was observed in the isothermal case.
- The directivity of the wavepacket source identified by the imaging is again superdirective, in agreement with the CS signatures identified by the POD and wavelet filtering operations performed in the previous sections.

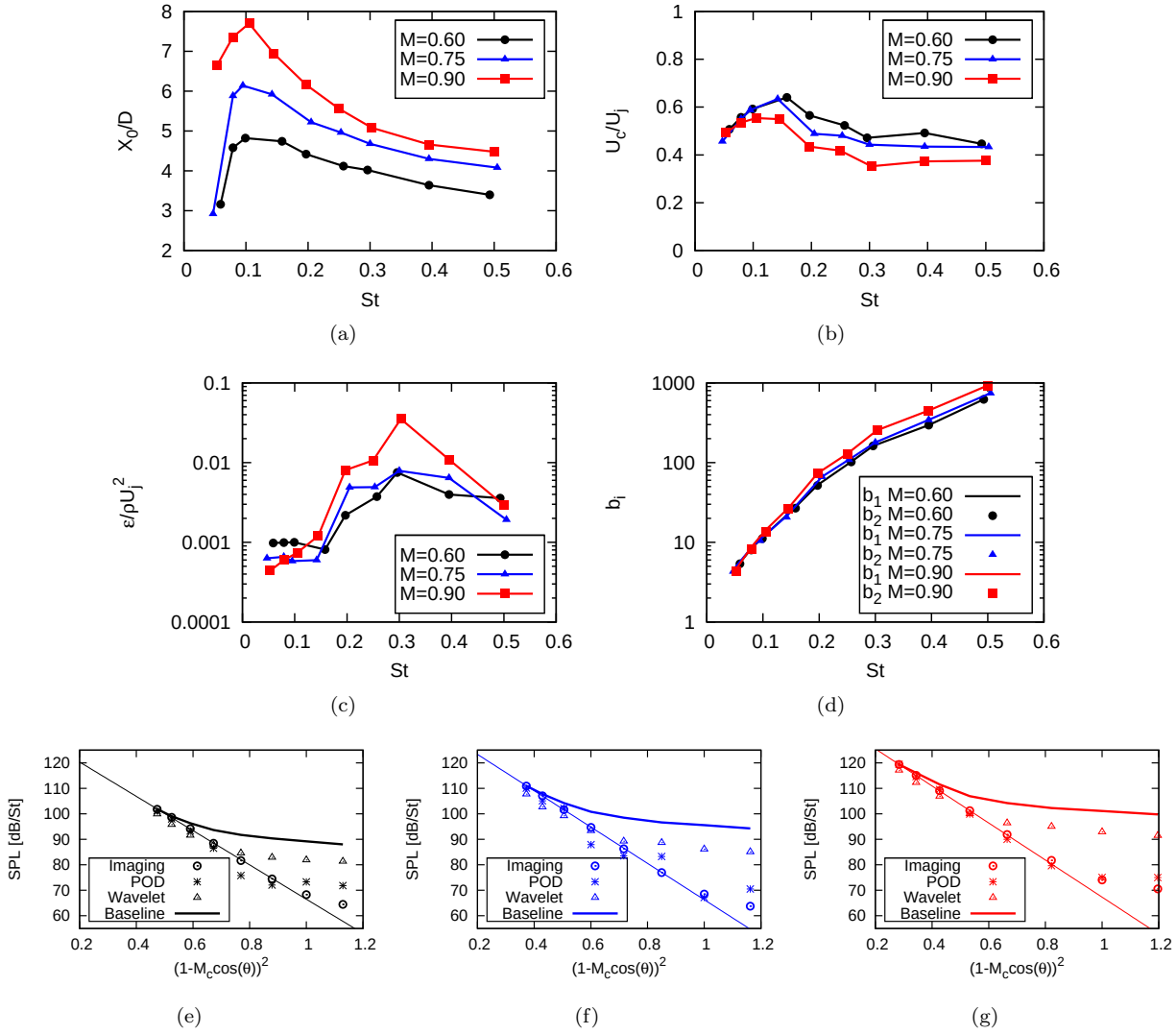

Figure 13. Wavepacket parameters, for isothermal jet, as a function of Strouhal and Mach number. (a) Wavepacket center; (b) convection velocity; (c) amplitude; (d) slopes. wavepacket superdirectivity: (e), (f) & (g) correspond to Mach 0.6, 0.75 and 0.9, respectively.

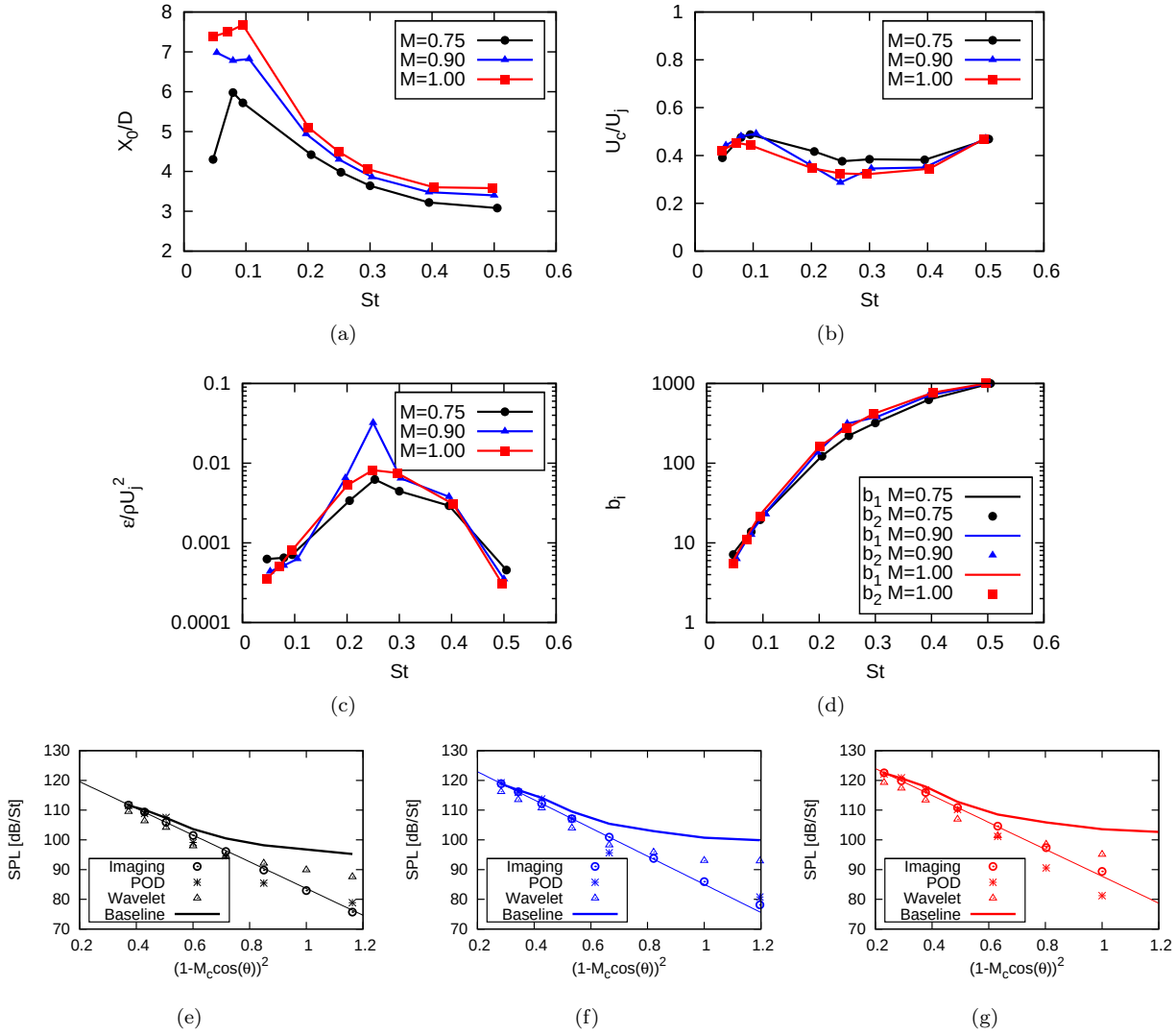

Figure 14. Wavepacket parameters, for heated jet, as a function of Strouhal and Mach number. (a) Wavepacket center; (b) convection velocity; (c) amplitude; (d) slopes. wavepacket superdirectivity: (e), (f) & (g) correspond to Mach 0.75, 0.9 and 1, respectively.

VII. Conclusion and future work

We have presented an analysis of the sound field radiated by jets at various Mach numbers and temperature ratio. POD is used to assess the spatial structure, wavelet transforms being used to study the temporal intermittency. Using each of these approaches, the sound field is decomposed into a component that we loosely associate with coherent structures (CS), and a residuum (R). Both of these operations lead to filtered fields consistent with wavepacket radiation[2]

A difference in the source compactness of the heated and isothermal flows is observed in the switch from Helmholtz to Strouhal scaling of the shallow-angle spectra as the jet is heated. In addition to this, we find that while the intermittency of the sound field radiated by isothermal jets is insensitive to changes in Mach number, in heated jets the intermittency decreases as the Mach number is increased.

Finally, application of a source imaging algorithm allows the dependence of the wavepacket parameters on Mach number and temperature to be assessed. The trends identified are consistent with known changes in the mean flow and known results of linear stability analysis.

Acknowledgments

The present work was initiated during the 3^{rd} IFFC held in Poitiers in 2008. It was supported by SNECMA and CNPq, National Council of Scientific and Technological Development - Brazil.

References

[1]Kœnig, M., Cavalieri, A. V. G., Jordan, P., Delville, J., Gervais, Y., Papamoschou, D., Samimy, M., and Lele, S., "Farfield filtering and source imaging for the study of jet noise," No. 2010-3779, 16th AIAA/CEAS Aeroacoustics Conference (31st AIAA Aeroacoustics Conference), Stockholm, Sweden, June 6-9 2010.

[2]Cavalieri, A. V. G., Jordan, P., Agarwal, A., and Gervais, Y., "Jittering wave-packet models for subsonic jet noise," to appear in Journal of Sound and Vibration, 2011.

[3]Tam, C., Golebiowski, M., and Seiner, J., "On the two components of trubulent mixing noixe from supersonic jets," No. 96-1716, 2nd AIAA/CEAS Aeroacoustics Conference (17th AIAA Aeroacoustics Conference), 1996.

[4]Bodony, D. and Lele, S., "Low-frequency sound sources in high-speed turbulent jets," Journal of Fluid Mechanics, Vol. 617, 2008, pp. 231–253.

[5]Juvé, D., Sunyach, M., and Comte-Bellot, G., "Intermittency of the noise emission in subsonic cold jets," Journal of Sound and Vibration, Vol. 71, 1980, pp. 319–332.

[6]Guj, G., Carley, R., and Camussi, C., "Acoustic identification of coherent structures in a turbulent jet," Journal of Sound and Vibration, Vol. 259, 2003, pp. 1037–1065.

[7]Hileman, J., Thurow, B., Carabello, E., and Samimy, M., "Large-scale structure evolution and sound emission in high-speed jets: real-time visualisation with simultaneous acoustic measurements," Journal of Fluid Mechanics, Vol. 544, 2005, pp. 277–307.

[8]Farge, M., "Wavelet transforms and their applications to turbulence," Annual Review of Fluid Mechanics, Vol. 24, 1992, pp. 395–458.

[9]Jordan, P. and Gervais, Y., "Modelling self- and shear-noise mechanisms in inhomogeneous, anisotropic turbulence," Journal of Sound and Vibration, Vol. 279, 2005, pp. 529–555.

[10]Torrence, C. and Compo, G., "A practical Guide to Wavelet Analysis," Bulletin of the American Meteorological Soc., Vol. 79, No. 1, 1998.

[11]Lush, P., "Measurements of subsonic jet noise and comparison with theory," Journal of Fluid Mechanics, Vol. 46, No. 3, 1971, pp. 477–500.

[12]Tanna, H., "An experimental study of jet noise Part I: Turbulent mixing noise," Journal of Sound and Vibration, Vol. 50, No. 3, 1977, pp. 405–428.

[13]Cavalieri, A. V. G., Jordan, P., Colonius, T., and Gervais, Y., "Axisymmetric superdirectivity in subsonic jets," 17th AIAA/CEAS Aeroacoustics Conference and Exhibit, Portland, OR, USA, June 5-8 2011.

[14]Crow, S., "Acoustic gain of a turbulent jet," Phys. Soc. Meeting, Univ. Colorado, Boulder, paper IE, Vol. 6, 1972.

[15]Crighton, D., "Basic principles of aerodynamic noise generation," Prog. Aerospace Sci., Vol. 16, 1975.

[16]Ffowcs-Williams, J. and Kempton, A., "The noise from the large-scale structure of a jet," Journal of Fluid Mechanics, Vol. 84, 1978, pp. 673–694.

[17]Crighton, D. and Huerre, P., "Shear layer pressure fluctuations and superdirective acoustic sources," Journal of Fluid Mechanics, Vol. 220, 1990, pp. 355–368.

[18]Papamoschou, D., "Imaging of directional ditributed noise sources," No. 2008-2885, 14th AIAA/CEAS Aeroacoustics Conference (29th AIAA Aeroacoustics Conference), 2008.

[19]Shanno, D. and Phua, K., "Minimization of Unconstrained Multivariate Functions," ACM Transactions on Math. Software, Vol. 6, No. 4, 1980, pp. 618–622.

[20]Morris, P., "A note on noise generation by large scale turbulent structures in subsonic and supersonic jets," International Journal of Aeroacoustics, Vol. 8, No. 4, 2009, pp. 301–315.

[21]Lau, J., Morris, P., and Fisher, M., "Measurements in subsonic and supersonic free jets using a laser velocimeter," Journal of Fluid Mechanics, Vol. 93, 1979, pp. 1–27.

[22]Michalke, A., "Survey on jet instability theory," Progress in Aerospace Sciences, Vol. 21, 1984, pp. 159–199.

[23]Papamoschou, D., "Initial efforts in wavepacket modeling of supersonic jet noise," General Lecture - International Forum on Flow Control - Poitiers, France, December 2008.